Theory of photonic crystal heterostructures

Emanuel Istrate, Mathieu Charbonneau-Lefort, and Edward H. Sargent

Department of Electrical and Computer Engineering, University of Toronto,
10 King's College Road, Toronto, Ontario, Canada, M5S 3G4

(Received 4 December 2001; published 29 August 2002)

We develop an envelope function formalism to describe the behavior of light inside a structure assembled out of dissimilar photonic band-gap materials. These photonic heterostructures are the optical analogs of quantum electronic heterostructures that make up resonant tunneling diodes and superlattices. We show that the behavior of these media is readily quantified and explained by reducing each constituent photonic band-gap material to a set of parameters related to the photonic crystals' dispersion relation, which are then used as inputs to an envelope equation. We also prove the validity of the approximation by comparison to full numerical simulations.

I. INTRODUCTION

Localization of light in certain strongly scattering dielectric media[1,2] has received extensive attention in recent years. In view of recent experimental demonstrations of a full photonic band gap inside large-scale infiltrated opals,[3] the predicted physical effects—suppressed spontaneous emission, improved laser performance, enhanced nonlinearity—may soon be realized.

The appealing analogy with the propagation and localization of electron waves inside electron-scattering media would suggest that the practical value of photonic crystals may lie not simply in their bulk properties, but in the realization of carefully differentiated structures of connected materials having different dispersion relations. The field of semiconductor quantum electronics relies on epitaxial growth of materials to realize functional devices such as resonant tunneling diodes and transistors, multiquantum well lasers, and intraband superlattice lasers.[4]

Semiconductor quantum heterostructures are understood quantitatively and qualitatively not through full solution of the Schrödinger equation inside each different superstructure, but instead by treating separately two distinct length scales on which electron wave behavior is manifested,[5] as illustrated in Fig. 1. First, bulk Bloch functions and the atomic potential energy seen by electrons inside constituent semiconductors are used to obtain the density of states and effective mass for a material. These embody the key consequences of the rapidly varying atomic potential shown in Fig. 1(a).

The behavior of the electronic envelope function is then considered inside the macroscopic (heterostructure) potential 1(b) formed by concatenations of the media whose bulk properties are now known. In the electronic case, this yields an effective Schrödinger equation in which the confining potential is determined by band offsets at the heterojunctions. The energy states of electrons in the heterostructure are then obtained from these equations, in which there remains no explicit dependence on the potential variations on the scale of the crystal lattice period. Phenomena accessible in this approximation include quantum-confined discrete quantum

well states; interband and intraband transition-matrix elements; resonant tunneling; and the formation of superlattice subbands.[6,7]

Photonic crystal heterostructures have been recently introduced and investigated through numerical simulation and via experiment.[8–12] The placement and spatial differentiation of self-organizing photonic crystals on a planar substrate has recently been demonstrated experimentally.[13] The behavior of light in stacking faults of self-assembled crystals has also been explored.[14] In view of the great promise of photonic band-gap superstructures to enable realization of functional photonic devices, we seek in the present work to develop a method, analogous to the electronic envelope function approach, for analyzing the key features of photonic heterostructure behavior.

II. THEORY

While our analysis of the photonic case is inspired by the analysis of semiconductor structures,[5] significant modifications must be made when, instead of the Schrödinger equation, the electromagnetic wave equation is employed,

$$[\nabla^2 + \omega^2 \mu \epsilon - \nabla(\nabla \cdot)]\mathbf{E} = 0. \tag{1}$$

In the equation above, the last term of the operator, $\nabla(\nabla \cdot \mathbf{E})$, is new when compared to the equation for the electron.
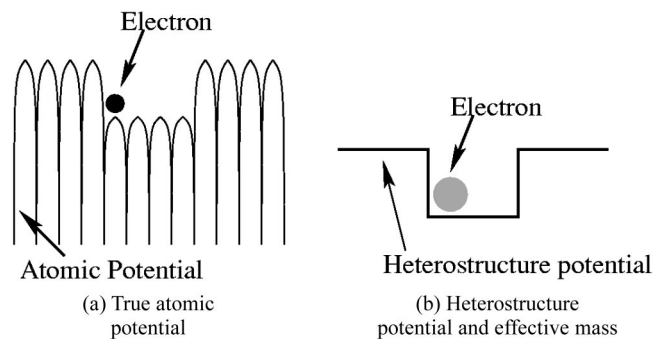

FIG. 1. Envelope approximation and effective mass in semiconductor structures.

It reflects the vectorial nature of the electromagnetic fields in the crystal.

A. The envelope equation

We separate the permittivity of the structure into a constant background component and two varying ones. The varying dielectric profiles describe the rapid variations, corresponding to the underlying photonic crystal, and the slower, confining, profile of the heterostructure, $\epsilon = \epsilon_b + \epsilon_v(\mathbf{r}) = \epsilon_b + \epsilon_f(\mathbf{r})[1 + \Delta_s(\mathbf{r})]$. These are included in the wave equation,

$$\{\nabla^2 + \omega_\lambda^2 \mu [\epsilon_b + \epsilon_v(\mathbf{r})] - \nabla(\nabla \cdot)\}\mathbf{E}_\lambda = 0. \quad (2)$$

The subscript λ is used to denote the frequency and the field of the heterostructure mode.

We assume that the heterostructure dielectric constant varies slowly enough that we can approximate the electric field with a linear superposition of the bulk Bloch modes, $\mathbf{E}_{n,\mathbf{k}} = \mathbf{u}_{n,\mathbf{k}}(\mathbf{r})e^{i\mathbf{k}\cdot\mathbf{r}}$,

$$\mathbf{E}_\lambda(\mathbf{r}) = \sum_{n,\mathbf{k}} \mathbf{E}_{n,\mathbf{k}}(\mathbf{r})\langle \mathbf{E}_{n,\mathbf{k}}|\mathbf{E}_\lambda\rangle, \quad (3)$$

where the sum is over all bands and all allowed wave vectors. The notation $\langle \mathbf{a}|\mathbf{b}\rangle$ is used to denote the projection of $\mathbf{b}$ onto $\mathbf{a}$, which is equivalent to the inner product of $\mathbf{a}$ and $\mathbf{b}$,

$$\langle \mathbf{a}|\mathbf{b}\rangle \equiv \int \mathbf{a}^*(\mathbf{r}) \cdot \mathbf{b}(\mathbf{r})d^3\mathbf{r}. \quad (4)$$

The Bloch functions $\mathbf{u}_{n,\mathbf{k}}$ can also be expanded in terms of the Bloch functions $\mathbf{u}_{n,\mathbf{k}_0}$ at a given vector $\mathbf{k} = \mathbf{k}_0$. Defining $\mathbf{u}_{m,\mathbf{k}_0} \equiv \mathbf{u}_m$ and $\langle \mathbf{u}_{m,\mathbf{k}_0}|\mathbf{u}_{n,\mathbf{k}}\rangle \equiv \langle m|n,\mathbf{k}\rangle$, we write

$$\mathbf{u}_{n,\mathbf{k}} = \sum_m \mathbf{u}_m(\mathbf{r})\langle m|n,\mathbf{k}\rangle. \quad (5)$$

It has been previously shown[15] that the above expansion must be done over all photonic crystal bands, but also over some unphysical solutions of the wave equation, which have zero frequency. Since in our later computations we will limit ourselves to a small number of bands, neighboring a band of interest, we will ignore the unphysical solutions, which only bring small corrections, as was pointed out.[15] Using these expansions, the electric field in the heterostructure may be expressed as

$$\mathbf{E}_\lambda(\mathbf{r}) = \sum_{m,\mathbf{k}} e^{i\mathbf{k}\cdot\mathbf{r}}W_{\lambda,m,\mathbf{k}}\mathbf{u}_m(\mathbf{r}), \quad (6)$$

where we have defined $W_{\lambda,m,\mathbf{k}} \equiv \sum_n \langle m|n,\mathbf{k}\rangle\langle \mathbf{E}_{n,\mathbf{k}}|\mathbf{E}_\lambda\rangle$. Using this expression in the wave Eq. (2), we obtain

$$\sum_{m,\mathbf{k}} W_{\lambda,m,\mathbf{k}}\{\nabla^2 + \omega_\lambda^2 \mu[\epsilon_b + \epsilon_v(\mathbf{r})] - \nabla(\nabla \cdot)\}e^{i\mathbf{k}\cdot\mathbf{r}}\mathbf{u}_m(\mathbf{r}) = 0. \quad (7)$$

In a bulk photonic crystal, the electromagnetic wave $\mathbf{E}_{m,\mathbf{k}_0} = \mathbf{u}_m e^{i\mathbf{k}_0\cdot\mathbf{r}}$ obeys the equation,

$$\{\nabla^2 + \omega_m^2 \mu[\epsilon_b + \epsilon_f(\mathbf{r})] - \nabla(\nabla \cdot)\}\mathbf{u}_m(\mathbf{r})e^{i\mathbf{k}_0\cdot\mathbf{r}} = 0. \quad (8)$$

Applying the operators in Eq. (7), simplifying and using Eq. (8), we obtain

$$\sum_{m,\mathbf{k}} W_{\lambda,m,\mathbf{k}}e^{i\mathbf{k}\cdot\mathbf{r}}\{-(k^2 - k_0^2) + 2i[(\mathbf{k} - \mathbf{k}_0) \cdot \nabla] - i(\mathbf{k} - \mathbf{k}_0)$$
$$\times(\nabla \cdot) - i\nabla[(\mathbf{k} - \mathbf{k}_0) \cdot] + \mathbf{k}(\mathbf{k}\cdot) - \mathbf{k}_0(\mathbf{k}_0\cdot) + (\omega_\lambda^2$$
$$- \omega_m^2)\mu[\epsilon_b + \epsilon_f(\mathbf{r})] + \omega_\lambda^2\mu\epsilon_f(\mathbf{r})\Delta_s(\mathbf{r})\}\mathbf{u}_m(\mathbf{r}) = 0. \quad (9)$$

In order to separate the length scale of the crystal from that of the heterostructure, it is useful to separate the position vector $\mathbf{r}$ into two components, $\mathbf{r} = \mathbf{R} + \boldsymbol{\rho}$. $\mathbf{R}$ gives the position of each unit cell of the crystal, while $\boldsymbol{\rho}$ describes positions inside each unit cell.

The separation of the position vector illustrates the idea of the envelope approximation. The vector $\boldsymbol{\rho}$ is associated with the rapidly varying dielectric profiles of the underlying photonic crystals. The vector $\mathbf{R}$, on the other hand, is used to denote variations that occur on a length scale much greater than that of the photonic crystal lattice. As such, the vector $\mathbf{R}$ labels variations associated with the heterostructure dielectric profile.

To solve Eq. (9) we project it along a given mode by multiplying it by $e^{-i\mathbf{k}'\cdot\mathbf{r}}\mathbf{u}_n^*(\mathbf{r})$ and integrating over the volume of the crystal. The following integrals were used in this evaluation:

$$I_1 = \int_{\text{crystal}} e^{i(\mathbf{k}-\mathbf{k}')\cdot\mathbf{r}}\mathbf{u}_n^* \cdot \mathbf{u}_m d^3\mathbf{r}$$
$$= \sum_{\mathbf{R}} e^{i(\mathbf{k}-\mathbf{k}')\cdot\mathbf{R}}\int_{\text{unit cell}} e^{i(\mathbf{k}-\mathbf{k}')\cdot\boldsymbol{\rho}}\mathbf{u}_n^* \cdot \mathbf{u}_m d^3\boldsymbol{\rho}. \quad (10)$$

The sum above is over all unit cells, and will be zero unless $\mathbf{k} = \mathbf{k}'$

$$I_1 = \delta_{\mathbf{k},\mathbf{k}'}\int \mathbf{u}_n^* \cdot \mathbf{u}_m d^3\boldsymbol{\rho} \equiv \delta_{\mathbf{k},\mathbf{k}'}u_{n,m}. \quad (11)$$

In a similar fashion, we obtain

$$I_2 = \int_{\text{crystal}} e^{i(\mathbf{k}-\mathbf{k}')\cdot\mathbf{r}}\mathbf{u}_n^* \cdot \epsilon_f(\mathbf{r})\mathbf{u}_m d^3\mathbf{r} = \delta_{\mathbf{k},\mathbf{k}'}\delta_{n,m}. \quad (12)$$

Here we have used the fact that Bloch modes in a photonic crystal are orthogonal with respect to the dielectric constant. The next parts of Eq. (9) are evaluated in a similar fashion. Special attention is paid to the term containing Δ_s

$$I_s = \int_{\text{crystal}} e^{i(\mathbf{k}-\mathbf{k}')\cdot\mathbf{r}} \mathbf{u}_n^* \cdot \epsilon_f(\mathbf{r})\Delta_s(\mathbf{r})\mathbf{u}_m d^3\mathbf{r}$$

$$\approx \sum_{\mathbf{R}} e^{i(\mathbf{k}-\mathbf{k}')\cdot\mathbf{R}}\Delta_s(\mathbf{R})\,\delta_{m,n} \equiv \Delta_{\mathbf{k}-\mathbf{k}'}^s\,\delta_{m,n}. \qquad (13)$$

After the integration, Eq. (9) becomes

$$\sum_m W_{\lambda,m,\mathbf{k}'}\left\{[-(k^2-k_0^2)+(\omega_\lambda^2-\omega_m^2)\mu\epsilon_b]u_{n,m}\right.$$

$$+\sum_{p=x,y,z}\sum_{q=x,y,z}(k_p'k_q'-k_{0,p}k_{0,q})\langle u_{n,k0,p}|u_{m,k0,q}\rangle$$

$$+[\kappa_{x,n,m}(k_x'-k_{0,x})+\kappa_{y,n,m}(k_y'-k_{0,y})+\kappa_{z,n,m}(k_z'$$

$$\left.-k_{0,z})]\right\}+\omega_\lambda^2\mu\sum_{\mathbf{k}}\Delta_{\mathbf{k}-\mathbf{k}'}^s W_{\lambda,n,\mathbf{k}}$$

$$+(\omega_\lambda^2-\omega_n^2)\mu W_{\lambda,n,\mathbf{k}'}=0. \qquad (14)$$

Here the variables p and q represent the direction variables x,y, and z in sequence. The following definitions were also made:

$$\kappa_{x,n,m}\equiv\left\langle\mathbf{u}_n\left|2i\frac{\partial}{\partial x}-i\boldsymbol{\nabla}(\hat{x}\cdot)-i\hat{x}(\boldsymbol{\nabla}\cdot)\right|\mathbf{u}_m\right\rangle$$

$$\equiv\int\mathbf{u}_n^*\left[2i\frac{\partial}{\partial x}-i\boldsymbol{\nabla}(\hat{x}\cdot)-i\hat{x}(\boldsymbol{\nabla}\cdot)\right]\mathbf{u}_m d^3\boldsymbol{\rho}, \quad (15)$$

$$\kappa_{y,n,m}\equiv\left\langle\mathbf{u}_n\left|2i\frac{\partial}{\partial y}-i\boldsymbol{\nabla}(\hat{y}\cdot)-i\hat{y}(\boldsymbol{\nabla}\cdot)\right|\mathbf{u}_m\right\rangle$$

$$\equiv\int\mathbf{u}_n^*\left[2i\frac{\partial}{\partial y}-i\boldsymbol{\nabla}(\hat{y}\cdot)-i\hat{y}(\boldsymbol{\nabla}\cdot)\right]\mathbf{u}_m d^3\boldsymbol{\rho}, \quad (16)$$

$$\kappa_{z,n,m}\equiv\left\langle\mathbf{u}_n\left|2i\frac{\partial}{\partial z}-i\boldsymbol{\nabla}(\hat{z}\cdot)-i\hat{z}(\boldsymbol{\nabla}\cdot)\right|\mathbf{u}_m\right\rangle$$

$$\equiv\int\mathbf{u}_n^*\left[2i\frac{\partial}{\partial z}-i\boldsymbol{\nabla}(\hat{z}\cdot)-i\hat{z}(\boldsymbol{\nabla}\cdot)\right]\mathbf{u}_m d^3\boldsymbol{\rho}. \quad (17)$$

In order to compute $W_{\lambda,n,\mathbf{k}'}$ for a specific band n, it is possible to express all other envelope functions $W_{\lambda,j,\mathbf{k}'}$, in terms of the envelope of band n, which are then inserted in Eq. (14). This would result in a single envelope equation, similar to the starting wave Eq. (1). This, however, is only possible for nondegenerate bands, since the equation will contain frequency differences between the different bands in the denominator. In this paper we will use a different method.

We take the inverse Fourier transform of Eq. (14) by multiplying by $e^{i\mathbf{k}'\cdot\mathbf{R}}$ and integrating over all $\mathbf{k}'$. The resulting equation is

$$\sum_m W_{\lambda,m}(\mathbf{R})\left[(\nabla^2+k_0^2-\omega_m^2\mu\epsilon_b)u_{n,m}\right.$$

$$+\sum_p\kappa_{p,n,m}\left(\frac{1}{j}\frac{\partial}{\partial p}-k_{0,p}\right)$$

$$\left.-\sum_p\sum_q\left(\frac{\partial^2}{\partial p\,\partial q}+k_{0p}k_{0q}\right)u_{n,p,m,q}\right]-\omega_n^2\mu W_{\lambda,n}(\mathbf{R})$$

$$=\sum_m W_{\lambda,m}(\mathbf{R})(-\omega_\lambda^2\mu\epsilon_b u_{n,m})$$

$$-\omega_\lambda^2\mu W_{\lambda,n}(\mathbf{R})[\Delta_s(\mathbf{R})+1]. \qquad (18)$$

Here again we use p and q to represent the directions x,y, and z. We have also defined $u_{n,p,m,q}\equiv\langle u_{n,k0,p}|u_{m,k0,q}\rangle$, where p and q select a single component of the Bloch vectors.

We can express the above equation in matrix form as follows:

$$\boldsymbol{\Theta}\mathbf{W}_\lambda(\mathbf{R})=\boldsymbol{\Phi}\omega_\lambda^2\mathbf{W}_\lambda(\mathbf{R}). \qquad (19)$$

Here $\mathbf{W}_\lambda$ is the column vector consisting of the elements $W_{\lambda,n}$. The elements of $\boldsymbol{\Theta}$ and $\boldsymbol{\Phi}$ are defined as

$$\Theta_{n,m}\equiv-\left\{(\nabla^2+k_0^2-\omega_m^2\mu\epsilon_b)u_{n,m}+\sum_p\kappa_{p,n,m}\left(\frac{1}{j}\frac{\partial}{\partial p}-k_{0p}\right)\right.$$

$$\left.-\sum_p\sum_q\left[\left(\frac{\partial^2}{\partial p\,\partial q}+k_{0,p}k_{0,q}\right)u_{n,p,m,q}\right]-\omega_n^2\mu\delta_{n,m}\right\},$$

$$(20)$$

$$\Phi_{n,m}\equiv\mu\epsilon_b u_{n,m}+\mu[\Delta_s(\mathbf{R})+1]\delta_{n,m}. \qquad (21)$$

Equation (19) describes the envelopes of the modes in a heterostructure. Knowledge of the matrix elements $u_{n,m},u_{n,p,m,q}$, and $\kappa_{p,n,m}$ allows calculation of the heterostructure modes and their frequencies.

If the photonic crystal properties vary very little over the entire heterostructure, we can assume this to be a small perturbation to the bulk crystal. This allows us to assume that matrix $\boldsymbol{\Theta}$ is constant everywhere, and the perturbation is given by the term $\Delta_s(\mathbf{R})$. For larger perturbations, this is no longer justified. In the case of abrupt heterojunctions, however, the matrices can be evaluated in each constant section of the crystal. The perturbative term Δ_s is then ignored, and the effect of the junction is reflected in the boundary conditions, discussed below, that need to be imposed.

In the remainder of this work we will consider an abrupt heterostructure that varies in the z direction only. We will set the background dielectric constant ϵ_b to zero. When Δ_s is not used a background constant can be included in ϵ_f. This reduces the heterostructure equation to

$$\boldsymbol{\Theta}\mathbf{W}_\lambda=\omega_\lambda^2\mu\mathbf{W}_\lambda. \qquad (22)$$

$$\Theta_{n,m} \equiv -\left[\left(\frac{\partial^2}{\partial z^2} + k_{0z}^2\right)(u_{n,m} - u_{n,z,m,z}) \right.$$

$$\left. + \kappa_{z,n,m}\left(\frac{1}{j}\frac{\partial}{\partial z} - k_{0z}\right) - \omega_n^2 \mu \delta_{n,m}\right]. \qquad (23)$$

The above equation is a second-order differential equation. Its solutions must therefore have an exponential form. We assume that their propagation vector will be close to our chosen vector $\mathbf{k}_0 = \hat{z}k_{0z}$.

$$\mathbf{W}_\lambda = \mathbf{W}_{\lambda,0}e^{i(k_{0z} + \delta k)Z}, \qquad (24)$$

$$\mathbf{GW}_{\lambda,0} = \omega_\lambda^2 \mu \mathbf{W}_{\lambda,0}, \qquad (25)$$

$$G_{n,m} = [(k_{0z} + \delta k)^2 - k_{0z}^2](u_{n,m} - u_{n,z,m,z})$$

$$- \kappa_{z,n,m}\delta k + \omega_n^2\mu\delta_{n,m}. \qquad (26)$$

We recognize this as a standard eigenvalue equation. In addition, for real δk, it can be shown that the matrix $\mathbf{G}$ is Hermitian. This ensures that the frequency eigenvalues will be real. This method allows calculation of the band structure of the bulk photonic crystal, if the modes are known at a single $\mathbf{k}$ vector.

Although the band structure of a crystal can be computed by other means, such as the plane-wave expansion method, the method developed here allows computation of the attenuation of a wave as a function of frequency inside the stop bands of the crystal. This is achieved by finding the energy eigenvalues corresponding to an imaginary propagation vector $\mathbf{k}$. Knowledge of the attenuation of a wave inside a crystal is essential in designing devices based on finite-sized crystals.

B. Boundary conditions

In order to study devices involving junctions between different photonic crystals, we need to find the conditions to be satisfied by the waves at the interfaces. We consider two crystals A and B with an interface perpendicular to the z direction located at $z=0$.

Since we are dealing with the envelope of an electric field, which is continuous, we assume that the envelope is also continuous across the interface,

$$\mathbf{W}_{\lambda,A}(0) = \mathbf{W}_{\lambda,B}(0). \qquad (27)$$

We note that this condition is different from the boundary conditions of continuous tangential electric- and magnetic-field components imposed by Maxwell's equations. Those conditions apply at the boundary between the materials forming the crystals, and are already incorporated in the Bloch modes that we use. Assuming that the two crystals forming the junction have the same embedding material, the heterointerface will not in general overlap with a material interface. We also assume that the first derivative of $\mathbf{W}_\lambda$ contains no infinite jumps. We now derive a boundary condition for the first derivative of the envelope function. We integrate Eq. (19) from $z=-\epsilon$ to $z=+\epsilon$, and take the limit of ϵ going to zero

$$\lim_{\epsilon \to 0}\int_{-\epsilon}^{\epsilon}\mathbf{\Theta W}_\lambda dz = \lim_{\epsilon \to 0}\omega_\lambda^2\int_{-\epsilon}^{\epsilon}\mathbf{\Phi W}_\lambda dz. \qquad (28)$$

The right-hand side of the equation contains a finite function, integrated over an interval going to zero. Hence it approaches zero. The equation can then be written as

$$\lim_{\epsilon \to 0}\int_{-\epsilon}^{\epsilon}\sum_m\left[\left(\frac{\partial^2}{\partial z^2} + k_{0z}^2\right)(u_{n,m} - u_{n,z,m,z})\right.$$

$$\left. + \kappa_{z,n,m}\left(\frac{1}{j}\frac{\partial}{\partial z} - k_{0z}\right)\right]W_{\lambda,m} - \omega_n^2\mu W_{\lambda,n}dz = 0.$$
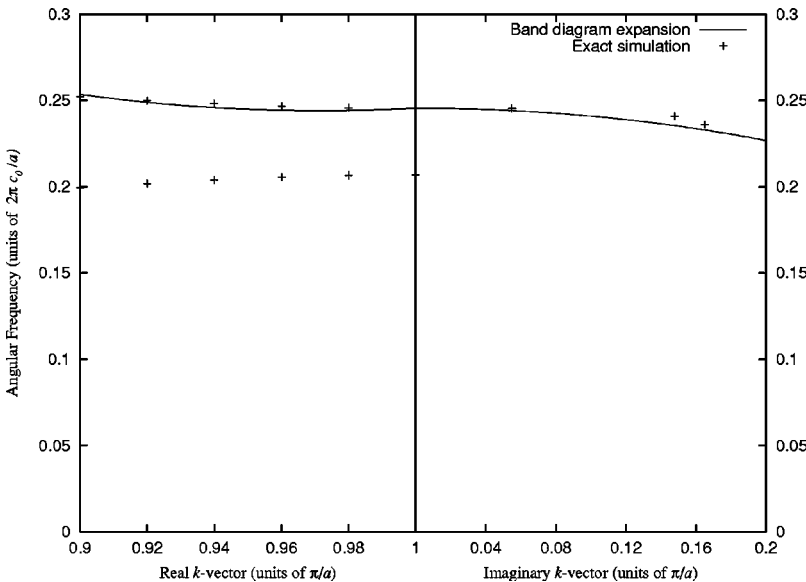
$$(29)$$

FIG. 2. Band diagram for a bulk crystal of silicon spheres in air, comparing the results of our expansion and exact simulations.

(a) Superlattice geometry

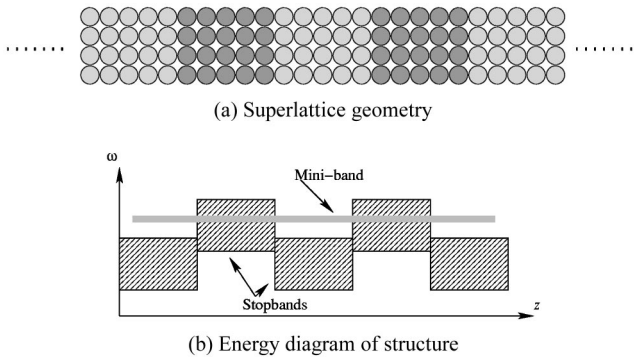(b) Energy diagram of structure

FIG. 3. Photonic crystal superlattice.

Since we have assumed that the first derivative of W_λ contains no infinite jumps, the last two terms vanish in the limit. We are left with

$$\lim_{\epsilon \to 0} \sum_m \int_{-\epsilon}^{\epsilon} \frac{\partial^2}{\partial z^2} (u_{n,m} - u_{n,z,m,z}) W_{\lambda,m} dz = 0. \quad (30)$$

From this we obtain the boundary conditions for the derivative of the envelope to be

$$\sum_m (u_{n,m} - u_{n,z,m,z}) \frac{\partial}{\partial z} W_{\lambda,m} = \text{const.} \quad (31)$$

This establishes a boundary condition for the derivative of the envelope across a heterojunction, similar to the boundary condition for electrons in the semiconductor case.[16] The parameters $u_{n,m} - u_{n,z,m,z}$ play the same role as the effective mass of electrons.

III. NUMERICAL EXAMPLE

We now present results obtained using the envelope approximation. The photonic crystals considered are composed of an array of spheres, arranged in a cubic structure. The heterostructures are made by varying the index of refraction of the spheres. The Bloch modes of the bulk crystals, needed by our method, are computed using the MIT *photonic bands* (MPB) program.[17] Using the envelope approximation, we have computed the dispersion relation for the second band near the edge of the Brillouin zone, as well as the imaginary propagation vectors in the stop band. The results are shown in Fig. 2 together with the true band diagram and attenuation constants obtained from Refs. 11 and 17. The agreement between our approximation and the true bands is good both for real and imaginary propagation vectors.

We now apply the theory developed above to a specific illustrative photonic crystal heterostructure. We consider the superlattice shown in Fig. 3(a). The structure consists of two alternating photonic crystals. The two crystal types have different band edges, shown in Fig. 3(b). As is the case with semiconductor superlattices, one or several allowed minibands are expected to appear for frequencies that are forbidden in one of the two regions. We refer to the regions of the structure where the wave is forbidden as the *barriers* and the regions of allowed propagation as the *wells*.
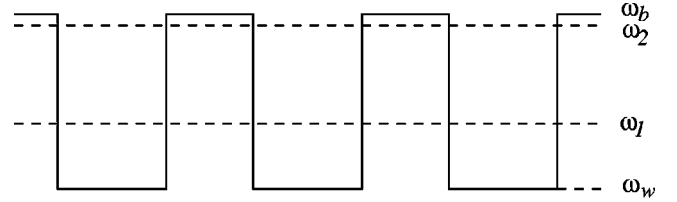

FIG. 4. Superlattice minibands computed with envelope approximation and with complete simulations.

We use the bands plotted in Fig. 2 together with $u_{n,m}$ and $u_{n,z,m,z}$ to compute the positions of the minibands in the structure. The barriers consist of spheres of dielectric constant $\epsilon = 10$, whereas the wells have $\epsilon = 11.56$. This will produce the band offset shown in Fig. 3(b). The width of the wells, b, was chosen to be 4 lattice constants, a. The barriers have a width c of 5 lattice constants. To find the positions of the minibands, we employ the technique described in the Appendix. With reference to Fig. 4, the band-edge frequencies of the well and barrier are $\omega_w = 0.245$, $\omega_b = 0.260$. The miniband appears between $\omega_1 = 0.252$ and $\omega_2 = 0.260$. All angular frequencies are given in units of $2\pi c_0/a$. We have also computed the position of the miniband using a full MPB simulation. It appears between $\omega_1 = 0.252$ and $\omega_2 = 0.258$. It should be noted that for this calculation we need the dispersion relations of the bulk materials; the attenuation constants in the stop band; and the boundary conditions. For the dispersion relation, we have the option of using the exact bands calculated using MPB or those calculated for the envelope approximation. We use in this example the exact band structure since it is precise and available. For the attenuation coefficients inside the stop band, we use the values obtained in the envelope approximation.

From these results, we conclude that the frequency position of the lower edge of the miniband is obtained with a high precision of 0.02% in the envelope approximation developed herein. The upper edge is off from its exact value by 0.8%—a result of the fact that the parameters $u_{n,m}$ and $u_{n,z,m,z}$ are computed for a propagation vector $k_{0,z} = \pi/a$. At the high frequencies at the top of the miniband, the propagation vector in the well is not very close to $k_{0,z}$.

IV. CONCLUSIONS

We have shown that the envelope function approximation can be applied to photonic crystal heterostructures in a manner similar to its use in semiconductor structures. The key aspects of the constituent photonic crystals are included through knowledge of the bulk band structure in each region of photonic crystal. This allows us to focus in subsequent computation on the evolution of spectral features arising out of mesoscopic heterostructure properties, facilitating design and analysis and reducing the problem from one which is numerically onerous to one which is readily tractable. The comparison to full numerical simulations described herein confirms the validity of the envelope approximation.
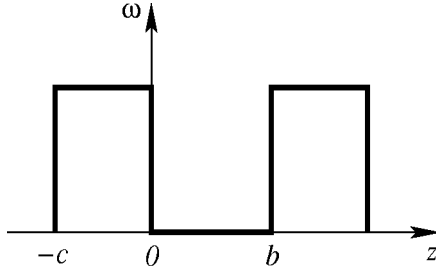
FIG. 5. Geometry used to find minibands.

APPENDIX: COMPUTATION OF MINIBAND POSITIONS

In this Appendix we describe the method used to compute the minibands of the superlattice considered in Sec. III.

Since we are working with waves close the the $k_{0,z}$ vector, we express the envelope of the waves as $\mathbf{W}_\lambda = \mathbf{V}_\lambda e^{jk_{0,z}z}$. $\mathbf{V}_\lambda$ represents the envelope with the oscillation at $k_{0,z}$ removed. Its boundary conditions require that $\mathbf{V}_\lambda$ and $\Sigma_m t_{n,m}(d/dz + k_{0,z})V_{\lambda,m}$ be continuous. Here we have defined $u_{n,m} - u_{n,z,m,z} \equiv t_{n,m}$.

We use a treatment similar to the Kronig–Penney model, using the arrangement in Fig. 5. Since we have a periodic structure, our solution must take the form of a Bloch function,

$$\mathbf{V}_\lambda(b) = \mathbf{V}_\lambda(-c)e^{jq(b+c)}, \tag{A1}$$

with q being the Bloch propagation vector.

It should be noted that the matrix elements $t_{n,m}$ have very few nondiagonal elements. By using an expansion around the first two nondegenerate bands only, we can eliminate the need to consider the sum of multiple modes in the envelope representation. We represent the mode in each section as the superposition of a forward and a backward propagating wave,

$$V_{\lambda,1} = A e^{jk_1 z} + B e^{-jk_1 z} \quad -c \leq z \leq 0, \tag{A2}$$

$$V_{\lambda,2} = C e^{jk_2 z} + D e^{-jk_2 z} \quad 0 \leq z \leq b. \tag{A3}$$

k_1 and k_2 represent the propagation vectors in the two sections of the superlattice. They are either real or imaginary, depending on whether propagation is allowed or forbidden in those sections. The propagation vectors are a function of frequency and can be found using the methods described in Sec. II A. In addition, for real propagation vectors, they can be computed using any program that can find the dispersion relations in a photonic crystal.

Applying the boundary and the Bloch conditions, Eq. (A1), at two points in the superlattice, we obtain a set of four equations for the coefficients A, B, C, and D. These equations can be presented in matrix form below

$$\mathbf{M} = \begin{bmatrix} 1 & 1 & 1 & 1 \\ t_1(k_1+k_0) & t_1(-k_1+k_0) & t_2(k_2+k_0) & t_2(-k_2+k_0) \\ e^{-jk_1c}e^{jq(b+c)} & e^{jk_1c}e^{jq(b+c)} & e^{jk_2b} & e^{-jk_2b} \\ t_1(k_1+k_0)e^{-jk_1c}e^{jq(b+c)} & t_1(-k_1+k_0)e^{jk_1c}e^{jq(b+c)} & t_2(k_2+k_0)e^{jk_2b} & t_2(-k_2+k_0)e^{-jk_2b} \end{bmatrix}. \tag{A4}$$

This set of equations has a nonzero solution only if its determinant is zero. This forms the condition for the appearance of minibands

$$\det(\mathbf{M}) = 0. \tag{A5}$$

[1] S. John, Phys. Rev. Lett. **58**, 2486 (1987).

[2] E. Yablonovitch, Phys. Rev. Lett. **58**, 2059 (1987).

[3] A. Blanco, E. Chomski, S. Grabtchak, M. Ibisate, S. John, S. W. Leonard, C. Lopez, F. Meseguer, H. Miguez, J. P. Mondia, G. A. Ozin, O. Toader, and H. M. van Driel, Nature (London) **405**, 437 (2000).

[4] G. Scamarcio, F. Capasso, C. Sirtori, J. Faist, A. L. Hutchinson, D. L. Sivco, and A. Y. Cho, Science **276**, 773 (1997).

[5] W. W. Chow and S. W. Koch, *Semiconductor-Laser Fundamentals: Physics of the Gain Materials* (Springer, New York, 1999).

[6] C. Weisbuch and B. Vinter, *Quantum Semiconductor Structures: Fundamentals and Applications* (Academic Press, Boston, 1991).

[7] L. Coldren and S. W. Corzine, *Diode Lasers and Photonic Integrated Circuits* (Wiley, New York, 1995).

[8] P. Jiang, N. Ostojic, R. Narat, D. M. Mittleman, and V. L. Colvin, Adv. Mater. **13**, 389 (2001).

[9] S. Yano, Y. Segawa, J. S. Bae, K. Mizuno, H. Miyazaki, S. Yamaguchi, and K. Ohtaka, in *International Workshop on Photonic and Electromagnetic Crystal Structures*, edited by O. Hanaizumi (RIEC, Sendai, Japan, 2000), pp. W4–10.

[10] E. Istrate and E. H. Sargent, in *International Workshop on Photonic and Electromagnetic Crystal Structures*, edited by O. Hanaizumi (RIEC, Sendai, Japan, 2000), pp. T4–16.

[11] N. Stefanou, V. Yannopapas, and A. Modinos, Comput. Phys. Commun. **113**, 49 (1998).

[12] C. Zhang, F. Qiao, and J. Wan, J. Appl. Phys. **87**, 3174 (2000).

[13] E. Kumacheva, R. Golding, M. Allard, and E. H. Sargent, Adv. Mater. **14**, 221 (2002).

[14] V. Yannopapas, N. Stefanou, and A. Modinos, Phys. Rev. Lett. **86**, 4811 (2001).

[15] J. E. Sipe, Phys. Rev. E **62**, 5672 (2000).

[16] I. Galbraith and G. Duggan, Phys. Rev. B **38**, 10 057 (1988).

[17] S. G. Johnson and J. D. Joannopoulos, Opt. Express **8**, 173 (2001).